

IgCONDA-PET: Implicitly-Guided Counterfactual Diffusion for Detecting Anomalies in PET Images

Shadab Ahamed^{1,2}, Yixi Xu³, and Arman Rahmim^{1,2}

¹ University of British Columbia, Vancouver, BC, Canada

² BC Cancer Research Institute, Vancouver, BC, Canada

³ Microsoft AI for Good Research Lab, Redmond, WA, USA
shadabahamed1996@gmail.com

Abstract. Minimizing the need for pixel-level annotated data for training PET anomaly segmentation networks is crucial, particularly due to time and cost constraints related to expert annotations. Current un-/weakly-supervised anomaly detection methods rely on autoencoder or generative adversarial networks trained only on healthy data, although these are more challenging to train. In this work, we present a weakly supervised and *Implicitly guided COuN*terfactual diffusion model for *Detecting Anomalies in PET* images, branded as IgCONDA-PET. The training is conditioned on image class labels (healthy vs. unhealthy) along with implicit guidance to generate counterfactuals for an unhealthy image with anomalies. The counterfactual generation process synthesizes the healthy counterpart for a given unhealthy image, and the difference between the two facilitates the identification of anomaly locations.⁴

Keywords: Diffusion model · Anomaly detection · Implicit guidance

1 Introduction

Segmentation of cancerous anomalies from ¹⁸F-Fluorodeoxyglucose PET (¹⁸F-FDG PET) images is paramount to treatment planning and surgical intervention. Obtaining expert voxel-level annotation is time-consuming and prone to errors due to intra- and inter-observer variabilities. In regard to this, there is a growing interest towards weakly supervised medical anomaly detection, which rely on weak image-level labels instead of dense pixel-level labels for training. In this paper, we employ a weakly supervised diffusion probabilistic model (DPM) to perform pixel-level anomaly detection.

Related work. Unsupervised deep learning-based anomaly detection in PET images has been explored in [13,6,14], although these were developed on brain PET datasets for anomalies related to dementia. Moreover, these methods were trained only on healthy cases under the assumption that since the model is trained to reconstruct only healthy data, it would fail on unhealthy cases in

⁴ Code will be available at: <https://github.com/igcondapet/IgCONDA-PET.git>

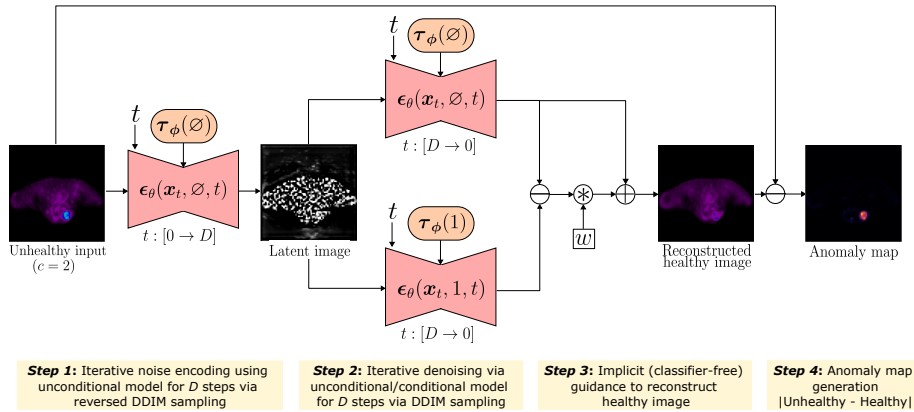


Fig. 1. IgCONDA-PET: Implicitly-guided counterfactual DPM sampling methodology for domain translation between an unhealthy image and its healthy counterfactual for PET. The anomaly map is defined as the absolute difference between the unhealthy and corresponding reconstructed healthy image.

the regions of anomalies, thereby highlighting the unhealthy areas. Despite this simple idea, these models might not work well in practice because a lesion would deform regions around it and these deformations should not be captured by the anomaly detection algorithm. Moreover, as shown in [4,21], detecting anomalies without being shown examples of unhealthy data is non-trivial and such models often simply highlight regions of hyper-intensity in the image. Recently, diffusion models have been employed for medical anomaly detection [26,21], but these have largely been validated only on brain MRI datasets alone. PET-based application of diffusion models have been explored in the context of image denoising [11,27] and reconstruction [12,28], although their application to anomaly detection, especially in oncological PET use-cases, have been limited [9].

In this work, we propose a counterfactual DPM based on [21], trained on healthy and unhealthy axial PET slices with image-level labels. The class labels were preprocessed using an embedding module and were then fed into each level of the model augmented with attention mechanism [20] (Sec. 2.2). During inference, the synthesis process can be controlled via class labels and the anomalies were highlighted by conducting minimal intervention (known as counterfactual generation [22]) to perform an unhealthy to healthy domain translation. We then generate heatmaps by computing the difference between the unhealthy image and its reconstructed healthy counterfactual (Sec. 2.3).

Contributions. To the best of our knowledge, this is the first work on (i) counterfactual DPM for PET anomaly detection, pertaining to four distinct cancer phenotypes. We (ii) train our models using implicit guidance (Sec. 2.1), which eliminates the reliance on a downstream classifier for guidance [26]; (iii) conduct extensive ablation studies with respect to the presence or absence of attention mechanism within the different layers of DPM (Sec. 2.2); (iv) perform exper-

iments highlighting the sensitivity of the method to different hyperparameter choices; (v) show the superiority of our method against several other related state-of-the-art methods for weakly-supervised anomaly detection using the optimal Dice similarity coefficient (DSC), lesion SUV_{max} detection sensitivity, and 95%tile Hausdorff distance (HD95) metrics.

2 Method

The diffusion models consists of a forward (noising) and a reverse (denoising) process. The forward process is a fixed Markovian process that iteratively adds Gaussian noise to the input image $x_0 \sim p_{\text{data}}$ following a variance schedule $\beta_1, \beta_2, \dots, \beta_T$ for time steps $t \in \{1, \dots, T\}$. Using the reparametrization trick [15], the forward process of sampling x_t can be expressed in terms of x_0 at any arbitrary time step t in closed form as $q(x_t|x_0) = \mathcal{N}(x_t; \sqrt{\bar{\alpha}_t}x_0, (1 - \bar{\alpha}_t)\mathbb{1})$, where $x_t = \sqrt{\bar{\alpha}_t}x_0 + \sqrt{1 - \bar{\alpha}_t}\epsilon$, $\alpha_t = 1 - \beta_t$, $\bar{\alpha}_t = \prod_{s=1}^t \alpha_s$ and $\epsilon \sim \mathcal{N}(0, \mathbb{1})$.

The denoising process p_θ is learned using a conditional denoising UNet denoted by $\epsilon_\theta(x_t, c, t)$ [20,21], with embeddings for time t and class labels c , with $c \in \{\emptyset, 1, 2\}$. Here, \emptyset represents an unconditional class, while the labels 1 and 2 represent the healthy and unhealthy classes respectively. The learned reverse sampling process is given by $p_\theta(x_{t-1}|x_t) = \mathcal{N}(x_{t-1}; \mu_\theta(x_t, t), \beta_t\mathbb{1})$. During training, the model $\epsilon_\theta(x_t, c, t)$ is used to estimate the noise added to the noised input by optimizing MSE loss given by $\mathcal{L} = \mathbb{E} \left(\|\epsilon - \epsilon_\theta(x_t, c, t)\|_2^2 \right)$, where $\epsilon \sim \mathcal{N}(0, \mathbb{1})$. We utilize the deterministic sampling from the denoising diffusion implicit model (DDIM) [24] to estimate x_{t-1} from x_t given by,

$$x_{t-1} = \sqrt{\bar{\alpha}_{t-1}} \left(\frac{x_t - \sqrt{1 - \bar{\alpha}_t} \cdot \epsilon_\theta(x_t, c, t)}{\sqrt{\bar{\alpha}_t}} \right) + \sqrt{1 - \bar{\alpha}_{t-1}} \cdot \epsilon_\theta(x_t, c, t) \quad (1)$$

2.1 Implicit guidance (Ig)

The data in this work consists of slices that are either healthy (with no lesion, denoted by label $c = 1$) or unhealthy (with one or more lesions, denoted by $c = 2$). We use implicit guidance (Ig) (also referred to as classifier-free guidance) [16], where a single model is jointly trained on unconditional and conditional objectives by randomly setting p_{uncond} proportion of input labels in each batch to \emptyset (implemented using $c = 0$). Here, we set $p_{\text{uncond}} = 15\%$ [16]. This procedure forces the model to learn to generate samples even in the absence of conditioning based on one of the classes from the data. As a result, the training objective gives rise to $\epsilon_\theta(x_t, \emptyset, t)$ and $\epsilon_\theta(x_t, c, t)$ representing the unconditional and conditional predictions respectively. During inference, sampling with an intervention to the conditioning c is performed using $\tilde{\epsilon}_\theta(x_t, c, t) = \epsilon_\theta(x_t, \emptyset, t) + w \cdot (\epsilon_\theta(x_t, c, t) - \epsilon_\theta(x_t, \emptyset, t))$, where w is referred to as the guidance scale [21,16].

2.2 Class conditioning via attention layers

The class conditioning in this work is implemented via conditional attention mechanism that has been shown to improve performance in [15,7,20,21]. We use an embedding layer $\tau_\phi(c)$ with trainable parameters ϕ , dictionary size of 3 and dimension $d = 64$ to project the class tokens c to vector representations. These vector representations are fed into the UNet augmented with attention layers at each levels. These attention modules implement,

$$\text{Attention}(Q, K_c, V_c) = \text{softmax}\left(\frac{QK_c^T}{\sqrt{d}}\right)V_c \quad (2)$$

where Q is the query matrix, and $K_c = \text{concat}[K, \tau_\phi(c)]$, and $V_c = \text{concat}[V, \tau_\phi(c)]$ are augmented key and value matrices respectively, where each of Q , K and V are derived from the previous convolutional layers [7]. The UNet consisted of 3 levels with 64 channels each and one residual block per level. Each level in UNet could incorporate attention mechanism with 16 channels per attention head and hence we denote our models using a 3-tuple (k_1, k_2, k_3) , where $k_i \in \{0, 1\}$ with 0 and 1 representing the absence or presence of attention mechanism in the i^{th} level respectively. We ablate over four different model types, namely, $(0, 0, 0)$, $(0, 0, 1)$, $(0, 1, 1)$, and $(1, 1, 1)$ to understand the effect of incorporating attention layers to anomaly detection performance. To the best of our knowledge, this is the first work based on counterfactual DPM studying the effect of attention mechanism in different levels of UNet on PET anomaly detection performance.

2.3 Counterfactual generation and anomaly detection

During inference, we first set a noise level $D \in \{1, \dots, T\}$ and a guidance scale w . Starting with an unhealthy input image x_0 (with $c = 2$), we perform noise encoding to obtain a latent image x_D by iteratively applying $\epsilon_\theta(x_t, \emptyset, t)$ using the reverse of Eq. (1). During the denoising process, a copy of generated x_D is fed into each of the $\epsilon_\theta(x_t, \emptyset, t)$ and $\epsilon_\theta(x_t, c = 1, t)$ (model with healthy conditioning) models and denoised for D steps via Eq. (1). The counterfactual (corresponding healthy image) is generated via Ig as described in Sec. 2.1. The absolute difference between the original input and the generated healthy counterfactual is computed to generate the anomaly map which can be used to obtain the location of anomalies. A schematic of the method has been shown in Fig. 1.

3 Experiments

Datasets. Two publicly-available and densely annotated oncological FDG PET datasets were used in this work, namely AutoPET [10] and HECKTOR [3]. The AutoPET dataset (n=1014) consisted of three cancer phenotypes, lymphoma, lung cancer, and melanoma, as well as healthy control patients, while the HECKTOR (n=524) consisted of patients presenting head & neck cancer. Both these datasets were pooled together and 1316, 88, and 104 cases were used for training,

validation and test phases. The test set excluded images from control patients. An additional 30 images were set aside for performing hyperparameter sensitivity experiments for finding the optimal noising steps D^* and guidance scale w^* . All 3D images were first resampled to the voxel spacing of AutoPET dataset, centrally cropped to a dimension of $192 \times 192 \times 288$ and normalized. This was followed by downsampling to dimension $64 \times 64 \times 96$. The axial slices of dimension 64×64 were extracted and labeled as healthy ($c = 1$) or unhealthy ($c = 2$) using the information from the voxel-level segmentation masks. All phases combined (excluding control patients), the fraction of slices with $c = 2$ was 15.6%.

Training. The parameters θ and ϕ of the 2D denoising UNet and the embedding layers for class conditioning respectively were trained using Adam optimizer with a learning rate of 10^{-5} . The model with the lowest validation MSE loss over 400 epochs was used for test set evaluation. During training, we set $T = 1000$ and batch size = 64. All experiments were done on a Microsoft Azure virtual machine with NVIDIA Tesla V100 GPUs with a collective GPU memory of 64 GiB and 448 GiB RAM. All implementations were done in Python 3.8.10, PyTorch 1.11.0, and MONAI 1.3.0 [19].

Benchmarks. The performance of our models, IgCONDA-PET(k_1, k_2, k_3), were compared against three other representative deep learning based weakly-supervised methods, namely (i) ResNet18-based slice classifier [1] with Grad-CAM explanations; (ii) f-AnoGAN [23], and (iii) DPM with classifier guidance (DPM+CG) [26]. Here, (ii) was trained only on healthy class, while the other two were trained on both healthy and unhealthy data. Apart from these, we used conventional method based on (iv) 41% SUV_{max} thresholding [18], and also trained a (v) IgCONDA-PET(1,1,1) on only healthy data (with evaluation performed unconditionally) as baselines, following past works in [21,4]. For fair comparison, all these methods were developed on 64×64 images, although most other training and inference hyperparameters were adapted from the original works and fine-tuned wherever necessary.

Evaluation metrics. We evaluated the anomaly detection performance using the mean of (i) optimal DSC obtained by sweeping over different values of thresholds on each of the anomaly maps [21]; (ii) detection sensitivity proposed as criterion 3 in [2] (at the same optimal threshold which maximized DSC), which considers an isolated anomaly prediction to be true positive iff it overlaps with the SUV_{max} pixel of the ground truth lesion; (iii) optimal HD95 (in pixels). Since we used patient-level SUV_{max} (in 3D) for 41% Thresholding, there were no segmentation for some of the slices via this method, and hence mean HD95 was not computed for this method, since it would be undefined for those slices.

4 Results and Discussion

Test set performance and comparison to other methods. We compare our method to other weakly-supervised and thresholding methods. As described in Sec. 2.2, we train our method in different settings for attention levels (k_1, k_2, k_3) and find that, in general, the presence of more attention layers at different levels

improves performance on all the three metrics across both datasets, as shown in Fig. 3 and Tab. 1. As compared to other methods, we show superior performance by our methods on AutoPET dataset on all metrics, beating f-AnoGAN by +5%, +0.2%, and -11.6 pixels on DSC, sensitivity, HD95, respectively. We also obtain the second best performance on the HECKTOR dataset on DSC and sensitivity metrics only falling behind f-AnoGAN by very small margins (-0.8% and -0.9%, respectively), although had a better performance on HD95 by -1.7 pixels. The performance of IgCONDA-PET(1,1,1) trained only on healthy data was much lower as compared to training on the entire data.

Table 1. Quantitative comparison between different anomaly detection methods on the test set. Performances of the top two models in each column has been shown in bold. \pm indicates standard deviation across all unhealthy slices. Here, *: “not trained”, †: “trained on only healthy data”, and ‡: “trained on both healthy and unhealthy data”.

Methods	Optimal DSC (\uparrow)		Lesion SUVmax detection sensitivity(\uparrow)		Optimal HD95(\downarrow)	
	AutoPET	HECKTOR	AutoPET	HECKTOR	AutoPET	HECKTOR
Thresholding* [18]	9.0 \pm 17.8	28.1 \pm 32.8	21.7 \pm 37.4	38.5 \pm 43.8	—	—
Classifier ‡ [1] + GradCAM*	30.2 \pm 23.7	25.6 \pm 18.0	65.8 \pm 36.9	70.0 \pm 35.6	17.8 \pm 13.8	12.6 \pm 6.6
f-AnoGAN † [23]	44.7 \pm 28.1	56.5\pm27.8	87.9\pm22.3	87.6\pm22.4	23.9 \pm 18.7	11.6 \pm 12.5
DPM+CG ‡ [26]	22.7 \pm 24.7	33.6 \pm 32.6	65.9 \pm 40.6	77.6 \pm 33.0	19.1 \pm 10.6	15.1 \pm 9.6
IgCONDA-PET(0,0,0) ‡	35.1 \pm 24.1	40.5 \pm 29.5	77.4 \pm 34.0	81.1 \pm 29.6	20.2 \pm 11.3	16.0 \pm 9.9
IgCONDA-PET(0,0,1) ‡	41.2 \pm 24.7	46.3 \pm 28.2	81.6 \pm 30.3	84.9 \pm 25.3	17.6 \pm 11.4	13.8 \pm 9.4
IgCONDA-PET(0,1,1) ‡	49.7\pm24.0	50.5 \pm 29.3	87.1 \pm 24.5	84.2 \pm 26.6	12.3\pm10.5	9.9\pm8.3
IgCONDA-PET(1,1,1) ‡	49.5\pm25.1	55.7\pm28.4	88.1\pm23.4	86.7\pm23.4	14.2\pm12.6	10.1\pm10.4
IgCONDA-PET(1,1,1) †	27.0 \pm 16.0	12.7 \pm 14.4	82.0 \pm 30.8	69.5 \pm 40.3	26.2 \pm 11.9	21.4 \pm 7.8

It is important to note that since IgCONDA-PET is conditioned to generate healthy counterfactuals from unhealthy images, it effectively does so by reducing the overall intensity of the image in all regions, although the reduction is much more pronounced in regions of anomalies, as compared to healthy anatomical regions. This helps preserve the healthy anatomical regions, giving rise to more accurate anomaly maps. This makes our model superior to other methods since IgCONDA-PET also has the potential to generate healthy-looking PET images, which are often hard to obtain as patients are usually scanned when there is a possibility for anomalies. Of all the methods explored in this work, only DPM+CG has the potential for counterfactual generation, although it had one of the lowest performances among all the deep learning based methods on our dataset (despite extensive hyperparameter tuning). This method was often failing at generating faithful healthy counterfactuals using classifier guidance, giving rise to artifacts in normal anatomical regions leading to higher values in those normal regions on the anomaly maps, as shown in Fig. 2. Hence, we show

that using classifier-free guidance is superior on our datasets for counterfactual generation as compared to using an extra trained classifier for guidance.

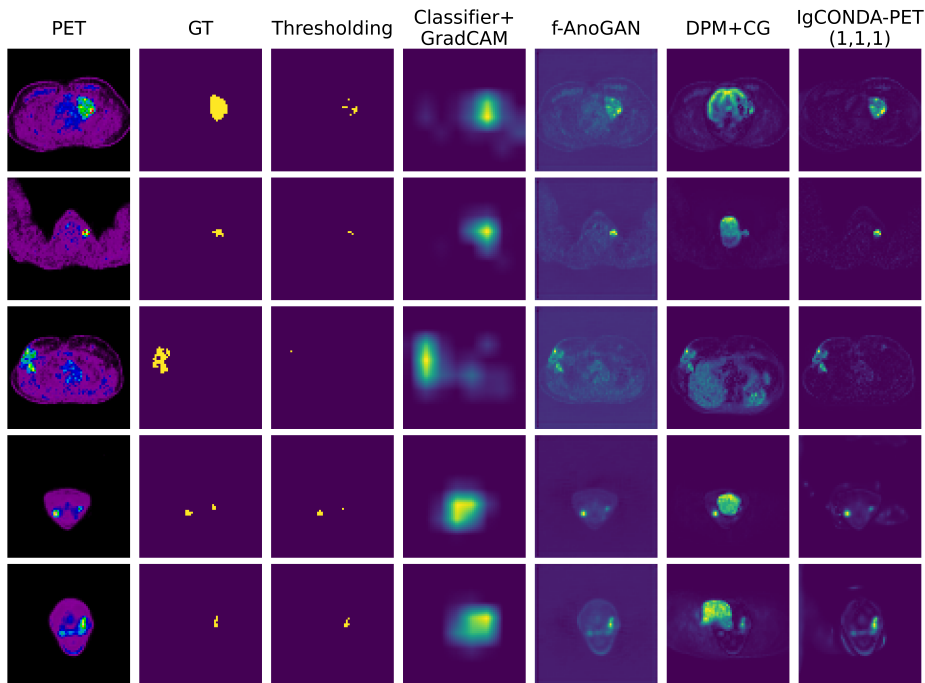


Fig. 2. Qualitative comparison between the anomaly maps generated by different methods on PET slices. GT represents the physician’s dense ground truth. Here, we set $D = 400$ and $w = 3.0$.

Sensitivity to inference hyperparameters. The best values for D and w were obtained after a series of ablation studies on a separate validation data consisting of 30 patients. As shown in Figs. 4 (a)-(e), the mean DSC across all threshold levels increases rapidly as a function of D for smaller values of D , while the best mean DSC (corresponding to the best threshold) plateaus for larger values of D (Fig. 4 (f)). From these experiments, we obtained the optimal values as $D^* = 400$ and $w^* = 3.0$, which were used for performing evaluations via Ig on all variants of our methods.

5 Conclusion

In this paper, we presented IgCONDA-PET, which is a weakly-supervised counterfactual generative diffusion method for pixel-level anomaly detection in PET images. We incorporated attention-based class conditioning and implicit guidance and show that both of these lead to better anomaly detection performance

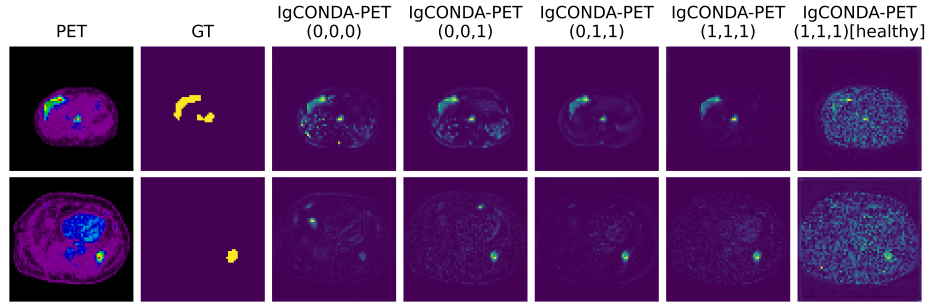


Fig. 3. Qualitative comparison between the anomaly maps generated by different variants of IgCONDA-PET showing the effect of the presence or absence of attention mechanism in different levels of DPM UNet. The last column shows the variant trained only on healthy data. Here, we set $D = 400$ and $w = 3.0$.

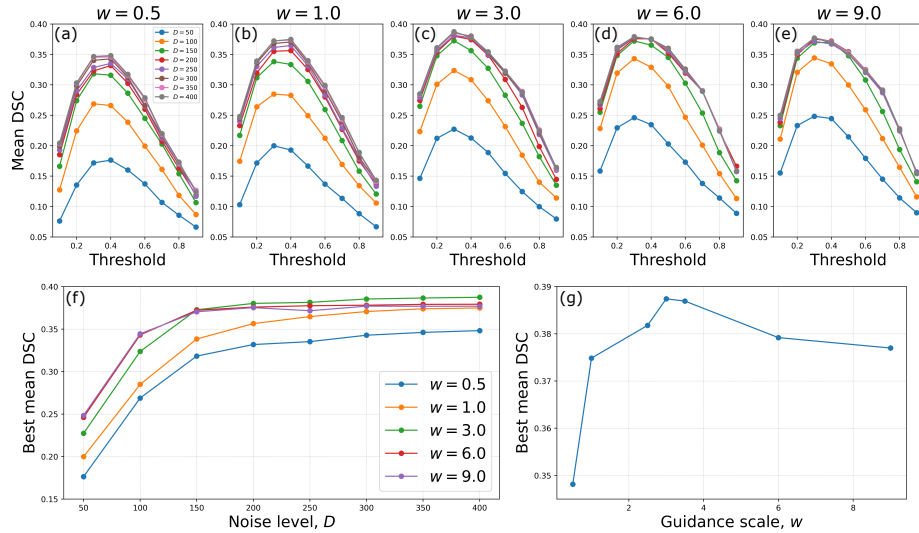


Fig. 4. (a)-(e) show trends for mean DSC values by sweeping over different thresholds for binarizing the anomaly maps for various values of noise levels D for five different values of w . (f) shows the trends for the best mean DSC as a function of noise level D for various w . (g) shows the best mean DSC as a function of w . All these experiments were performed for IgCONDA-PET(0,1,1) model.

on our PET datasets. Future work involves counterfactual generation of high-fidelity healthy PET datasets by incorporating anatomical information from CT images. We will also explore strategies for upscaling our methods to higher resolutions (in 2D) or training models directly on 3D datasets, which can be done by performing training on cropped patches [5,8], performing diffusion in a lower dimensional latent space [25], and better code and memory parallelism [17].

References

1. Ahamed, S., Xu, Y., Bloise, I., Joo, H., Uribe, C.F., Dodhia, R., Ferres, J.L., Rahmim, A.: A slice classification neural network for automated classification of axial pet/ct slices from a multi-centric lymphoma dataset. In: Medical Imaging 2023: Image Processing. vol. 12464, pp. 393–402. SPIE (2023)
2. Ahamed, S., Xu, Y., Gowdy, C., Bloise, I., Wilson, D., Martineau, P., Bénard, F., Yousefirizi, F., Dodhia, R., Lavista, J.M., et al.: Comprehensive evaluation and insights into the use of deep neural networks to detect and quantify lymphoma lesions in pet/ct images. arXiv preprint arXiv:2311.09614 (2023)
3. Andrearczyk, V., Oreiller, V., Boughdad, S., Rest, C.C.L., Elhalawani, H., Jreige, M., Prior, J.O., Vallières, M., Visvikis, D., Hatt, M., et al.: Overview of the hecktor challenge at miccai 2021: automatic head and neck tumor segmentation and outcome prediction in pet/ct images. In: 3D head and neck tumor segmentation in PET/CT challenge, pp. 1–37. Springer (2021)
4. Baur, C., Denner, S., Wiestler, B., Navab, N., Albarqouni, S.: Autoencoders for unsupervised anomaly segmentation in brain mr images: a comparative study. Medical Image Analysis **69**, 101952 (2021)
5. Bieder, F., Wolleb, J., Durrer, A., Sandkühler, R., Cattin, P.C.: Diffusion models for memory-efficient processing of 3d medical images. arXiv preprint arXiv:2303.15288 (2023)
6. Choi, H., Ha, S., Kang, H., Lee, H., Lee, D.S.: Deep learning only by normal brain pet identify unheralded brain anomalies. EBioMedicine **43**, 447–453 (2019)
7. Dhariwal, P., Nichol, A.: Diffusion models beat gans on image synthesis. Advances in neural information processing systems **34**, 8780–8794 (2021)
8. Ding, Z., Zhang, M., Wu, J., Tu, Z.: Patched denoising diffusion models for high-resolution image synthesis. In: The Twelfth International Conference on Learning Representations (2023)
9. Dong, Y., Gong, K.: Head and neck tumor segmentation from [18f] f-fdg pet/ct images based on 3d diffusion model. arXiv preprint arXiv:2401.17593 (2024)
10. Gatidis, S., Hepp, T., Früh, M., La Fougère, C., Nikolaou, K., Pfannenber, C., Schölkopf, B., Küstner, T., Cyran, C., Rubin, D.: A whole-body fdg-pet/ct dataset with manually annotated tumor lesions. Scientific Data **9**(1), 601 (2022)
11. Gong, K., Johnson, K., El Fakhri, G., Li, Q., Pan, T.: Pet image denoising based on denoising diffusion probabilistic model. European Journal of Nuclear Medicine and Molecular Imaging pp. 1–11 (2023)
12. Han, Z., Wang, Y., Zhou, L., Wang, P., Yan, B., Zhou, J., Wang, Y., Shen, D.: Contrastive diffusion model with auxiliary guidance for coarse-to-fine pet reconstruction. In: International Conference on Medical Image Computing and Computer-Assisted Intervention. pp. 239–249. Springer (2023)
13. Hassanaly, R., Brianceau, C., Colliot, O., Burgos, N.: Unsupervised anomaly detection in 3d brain fdg pet: A benchmark of 17 vae-based approaches. In: International

- Conference on Medical Image Computing and Computer-Assisted Intervention. pp. 110–120. Springer (2023)
14. Hassanaly, R., Brianceau, C., Solal, M., Colliot, O., Burgos, N.: Evaluation of pseudo-healthy image reconstruction for anomaly detection with deep generative models: Application to brain fdg pet. arXiv preprint arXiv:2401.16363 (2024)
 15. Ho, J., Jain, A., Abbeel, P.: Denoising diffusion probabilistic models. *Advances in neural information processing systems* **33**, 6840–6851 (2020)
 16. Ho, J., Salimans, T.: Classifier-free diffusion guidance. arXiv preprint arXiv:2207.12598 (2022)
 17. Li, M., Cai, T., Cao, J., Zhang, Q., Cai, H., Bai, J., Jia, Y., Liu, M.Y., Li, K., Han, S.: Distrifusion: Distributed parallel inference for high-resolution diffusion models. arXiv preprint arXiv:2402.19481 (2024)
 18. Novikov, M.: Multiparametric quantitative and texture 18 f-fdg pet/ct analysis for primary malignant tumour grade differentiation. *European Radiology Experimental* **3**, 1–8 (2019)
 19. Pinaya, W.H., Graham, M.S., Kerfoot, E., Tudosiu, P.D., Dafflon, J., Fernandez, V., Sanchez, P., Wolleb, J., da Costa, P.F., Patel, A., et al.: Generative ai for medical imaging: extending the monai framework. arXiv preprint arXiv:2307.15208 (2023)
 20. Ramesh, A., Dhariwal, P., Nichol, A., Chu, C., Chen, M.: Hierarchical text-conditional image generation with clip latents. arXiv preprint arXiv:2204.06125 **1**(2), 3 (2022)
 21. Sanchez, P., Kascenas, A., Liu, X., O’Neil, A.Q., Tsafaris, S.A.: What is healthy? generative counterfactual diffusion for lesion localization. In: *MICCAI Workshop on Deep Generative Models*. pp. 34–44. Springer (2022)
 22. Sanchez, P., Tsafaris, S.A.: Diffusion causal models for counterfactual estimation. arXiv preprint arXiv:2202.10166 (2022)
 23. Schlegl, T., Seeböck, P., Waldstein, S.M., Langs, G., Schmidt-Erfurth, U.: f-anogan: Fast unsupervised anomaly detection with generative adversarial networks. *Medical image analysis* **54**, 30–44 (2019)
 24. Song, J., Meng, C., Ermon, S.: Denoising diffusion implicit models. arXiv preprint arXiv:2010.02502 (2020)
 25. Vu Quoc, H., Tran Le Phuong, T., Trinh Xuan, M., Dinh Viet, S.: Lsegdiff: A latent diffusion model for medical image segmentation. In: *Proceedings of the 12th International Symposium on Information and Communication Technology*. pp. 456–462 (2023)
 26. Wolleb, J., Bieder, F., Sandkühler, R., Cattin, P.C.: Diffusion models for medical anomaly detection. In: *International Conference on Medical image computing and computer-assisted intervention*. pp. 35–45. Springer (2022)
 27. Xie, H., Gan, W., Zhou, B., Chen, X., Liu, Q., Guo, X., Guo, L., An, H., Kamilov, U.S., Wang, G., et al.: Dose-aware diffusion model for 3d ultra low-dose pet imaging. arXiv preprint arXiv:2311.04248 (2023)
 28. Xie, T., Cui, Z.X., Luo, C., Wang, H., Liu, C., Zhang, Y., Wang, X., Zhu, Y., Jin, Q., Chen, G., et al.: Joint diffusion: Mutual consistency-driven diffusion model for pet-mri co-reconstruction. arXiv preprint arXiv:2311.14473 (2023)

Supplementary Material

1 Additional examples comparing different variants of IgCONDA-PET (k_1, k_2, k_3)

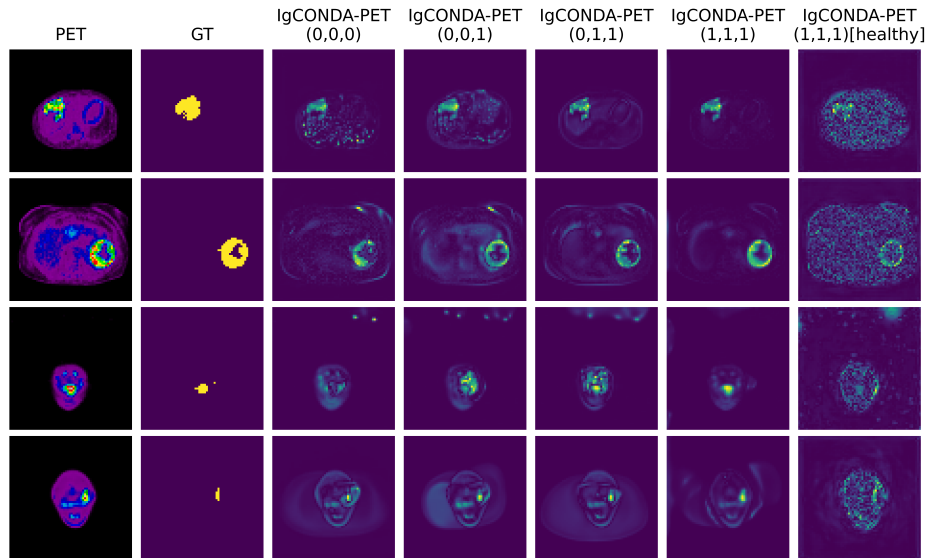


Fig. 5. Qualitative comparison between the anomaly maps generated by different variants of IgCONDA-PET. Here, we set $D = 400$ and $w = 3.0$ for all variants. The last column shows the variant trained only on healthy data.

2 Additional examples comparing IgCONDA-PET to other methods

(see next page)

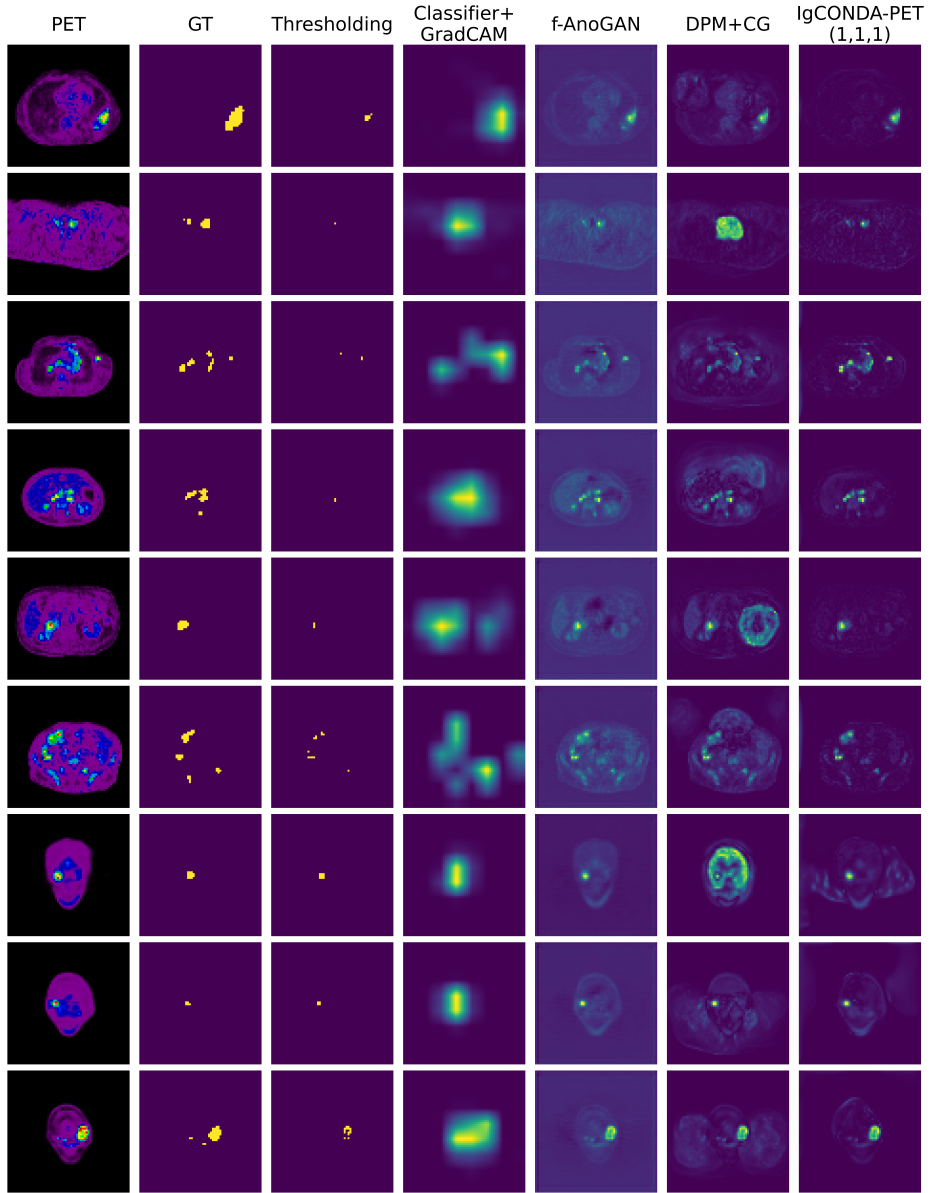


Fig. 6. Qualitative comparison between anomaly maps generated by different methods. Here, we set $D = 400$ and $w = 3.0$ for IgCONDA-PET(1,1,1).